# Effects of distortion of the intercluster motion in $^{2}$H, $^{3}$He, $^{3}$H, $^{6}$Li, and $^{9}$Be on Trojan horse applications

R. G. Pizzone,[1,2] C. Spitaleri,[1,2] A. M. Mukhamedzhanov,[3] L. D. Blokhintsev,[4] C. A. Bertulani,[5] B. F. Irgaziev,[6] M. La Cognata,[1,2] L. Lamia,[1,2] and S. Romano[1,2]

[1]*Laboratori Nazionali del Sud-INFN, Catania, Italy*

[2]*Dipartimento di Metodologie Fisiche e Chimiche per l'Ingegneria, Università di Catania, Catania, Italy*

[3]*Cyclotron Institute, Texas A&M University, College Station, USA*

[4]*Moscow State University, Moscow, Russia*

[5]*Physics Department, Texas A&M University, Commerce, USA*

[6]*GIK Institute of Engineering Sciences and Technology, Topi, District Swabi, N. W. F. P., Pakistan*

(Received 19 March 2009; published 31 August 2009)

Deuteron induced quasifree scattering and reactions have been extensively investigated in the past few decades as well as $^{6}$Li, $^{3}$H, $^{3}$He, and $^{9}$Be induced reactions. This was done not only for the investigation of nuclear structure and reaction mechanisms but also for important astrophysical applications (Trojan horse method). In particular the widths of the spectator momentum distributions in several nuclei, which have been used as Trojan horses, have been obtained as a function of the transferred momentum. Applications of Trojan horse method will also be discussed because the momentum distribution of the spectator particle inside the nucleus is a important input for this method. This gives hints on distortion effects at low energies important for nuclear astrophysics.

DOI: 10.1103/PhysRevC.80.025807 PACS number(s): 25.60.Gc, 26.20.−f, 21.10.Pc, 24.50.+g

## I. INTRODUCTION

The study of processes relevant for astrophysics involving light nuclei has considerably increased in the past decades due to the development of indirect methods trying to measure bare nucleus cross sections at astrophysically relevant energies. Among these methods we cite the Coulomb dissociation [1], the asymptotic normalization coefficient (ANC) [2–5], and the Trojan horse method (THM). The main features of this latter method are extensively discussed elsewhere [6–11]. Basically the THM allows us to measure the bare-nucleus two-body cross sections [or, equivalently, the bare-nucleus astrophysical $S(E)$ factors] by means of quasifree three-body reactions. The method is therefore an extension of excitation function measurements at energies above Coulomb barrier to reactions of astrophysical interest that take place at ultra-low energies [12,13]. In the standard THM the plane-wave impulse approximation (PWIA) is used, where the triple differential cross section for the Trojan horse (TH) reaction

$$A + x \rightarrow s + c + C \tag{1}$$

is factorized into two parts [see Eq. (3) below]. In such an approach, the Fourier transform of the bound-state wave function of the relative motion of the fragment $s$ and particle $x$ in the TH nucleus $a = (sx)$ can be eliminated by a simple procedure allowing us to extract the half-off-energy-shell (HOES) binary reaction cross section [see Eq. (3) below] that can be related with the on-energy-shell (OES) astrophysical factor. Nevertheless due to the presence of the other particles the momentum distribution of the spectator $s$ can be distorted thus having an impact on the final result.

The present article aims to estimate the distortion of the momentum distribution of the spectator $s$ based on the experimental data obtained in previous publications [7–33]. This will be performed by comparing the momentum distribution extracted in PWIA from experimental data with more elaborate momentum distribution calculation.

This task was already fulfilled for the case of the $\alpha$-$d$ clusters in $^{6}$Li. We have reanalyzed previous data from different experiments and we have compared our results with others present in literature. This study will also help to evaluate the dependence of the THM astrophysical factor on the full width at half maximum momentum (FWHM) distribution, which might introduce additional uncertainties to results obtained via this method. In Ref. [14] it was shown that errors introduced in the THM due to the momentum distribution uncertainties are much smaller than experimental errors caused by other sources. The present article will also help to point out the distortion effects that arise at low energies in the study of three-body processes and will suggest some way to bypass them in THM applications.

## II. TROJAN HORSE METHOD

Due to the difficulties of direct measurements of cross sections at astrophysical energies, alternative methods for determining bare nucleus cross sections of interest are needed. The THM is a unique and powerful tool that selects the quasifree (QF) contribution of an appropriate three-body reaction performed at energies well above the Coulomb barrier to extract a charged particle two-body cross section.

The basic idea of the THM [34] is to extract the cross section of an astrophysically relevant two-body reaction

$$A + x \rightarrow c + C \tag{2}$$

at low energies from a suitable three-body quasi-free reaction in Eq. (1) (see Fig. 1). This is done with the help of direct reactions theory assuming that the TH nucleus, $a$, has a dominant cluster component $(sx)$. In most applications (see

 

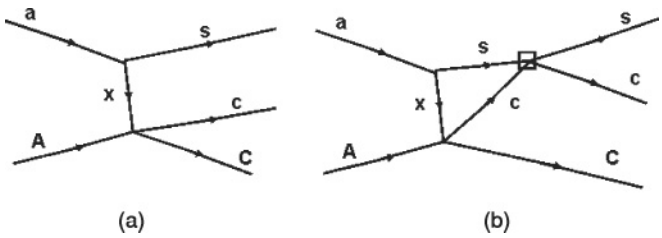


FIG. 1. (a): Pole diagram describing the quasifree mechanism; (b) the triangular diagram taking into account the final-state interaction as discussed in the text (a $c-C$ exchange in this diagram is equivalent).

Ref. [15] and references therein), this assumption is trivially fulfilled, e.g., $d=(pn)$. Particle $s$ is then considered to be spectator to the $A+x\rightarrow c+C$ reaction.

In the PWIA the cross section of the three-body reaction can be factorized into two terms and is given by [35]

$$\frac{d^3\sigma}{dE_c d\Omega_c d\Omega_C} \propto KF\left(\frac{d\sigma}{d\Omega}_{\text{c.m.}}\right)^{\text{HOES}} \cdot |\varphi(\mathbf{p_{sx}})|^2, \qquad (3)$$

where

(i) $[(d\sigma/d\Omega)_{\text{c.m.}}]^{\text{HOES}}$ is the HOES differential cross section for the two-body $A(x,c)C$ reaction at the relative $A$-$x$ energy $\text{E}_{\text{AX}}$ given in postcollision prescription by

$$E_{Ax}=E_{c-C}-Q_{2b}, \qquad (4)$$

$Q_{2b}$ is the two body $Q$ value of the $A+x\rightarrow c+C$ reaction and $E_{c-C}$ is the relative energy between the outgoing particles $c$ and $C$,

(ii) KF is a kinematical factor containing the final-state phase-space factor and it is a function of the masses, momenta, and angles of the particles [7],

(iii) $\varphi(\mathbf{p}_{sx})$ is the Fourier transform of the $a=(sx)$ bound state wave function $\varphi(\mathbf{r})$,

$$\varphi(\mathbf{p}_{sx})=(2\pi\hbar)^{-3/2}\int e^{-i\mathbf{p_{sx}}\cdot\mathbf{r}/\hbar}\varphi(\mathbf{r})d\mathbf{r}. \qquad (5)$$

and $\mathbf{p}_{sx}=\frac{m_x\mathbf{p}_s-m_s\mathbf{p}_x}{m_s+m_x}$ is the $s-x$ relative momentum and $\mathbf{p}_i$ and $m_i$ are the momentum and mass of the particle $i$. In the coordinate system, where $a$ is at rest, $\mathbf{p}_{sx}=\mathbf{p}_s$. If $|\varphi(\mathbf{p}_{sx})|^2$ is known and $KF$ is calculated, it is possible to derive $[(d\sigma/d\Omega)_{\text{c.m.}}]^{\text{HOES}}$ from a measurement of $d^3\sigma/dE_c d\Omega_c d\Omega_C$ by using Eq. (3).

$$\left(\frac{d\sigma}{d\Omega}\right)^{\text{HOES}} \propto \left(\frac{d^3\sigma}{dE_c d\Omega_c d\Omega_C}\right)\cdot[KF|\varphi(\mathbf{p}_s)|^2]^{-1}. \qquad (6)$$

In the experimental analysis the validity conditions of the impulse approximation (IA) appear to be fulfilled. It is worth noting that in the THM we are interested in the energy trend of the HOES binary reaction cross section $[(d\sigma/d\Omega)_{\text{c.m.}}]^{\text{HOES}}$ rather than in its absolute value. The latter can be extracted through normalization to the direct data available at higher energies.

The success of THM relies on the quasifree kinematics ($p_s\sim 0$ for nuclei in Table I), at which the TH conditions are best fulfilled. There were numerous works on the application of QF mechanism at low energies [19,24,32]. This simplified approach based on the PWIA in the QF kinematics was supported by the theory of the THM proposed by Baur ([34]), whose basic idea is to extract an $A+x\rightarrow C+c$ two-body reaction cross section at ultra-low energies from a suitable $A+a\rightarrow C+c+s$ quasifree three-body reaction. Under appropriate kinematical conditions, the three-body reaction is considered as the decay of the "Trojan horse" $a$ into the clusters $x$ and $s$ and the interaction of $A$ with $x$ inside the nuclear field, whereby the nucleus $s$ can be considered as a spectator during the reaction. Table I shows the TH nuclei used in several experiments; we focused our attention on nuclei with $l=0$ momentum for the relative $x$-$s$ motion. If the bombarding energy $E_A$ is chosen high enough to overcome the Coulomb barrier in the entrance channel of the reaction (2), both Coulomb barrier and electron screening effects are negligible.

TABLE I. Nuclei with cluster structure that can be used as Trojan horse nuclei and their principal properties.

| TH nucleus | Binding energy MeV | Clusters | Orbital momentum |
|---|---|---|---|
| $d$ | 2.225 | $p-n$ | $l=0$ |
| $t$ | 6.257 | $n-d$ | $l=0$ |
| $^3$He | 5.494 | $p-d$ | $l=0$ |
| $^6$Li | 1.475 | $\alpha$-$d$ | $l=0$ |
| $^9$Be | 2.467 | $\alpha$-$^5$He | $l=0$ |

In Ref. [34] it was proposed that the initial velocity of the projectile $A$ is compensated for by the Fermi motion of particle $x$ to obtain the binary cross section at astrophysical energies. In this framework, a momentum of the order of hundreds MeV/$c$ could be needed. However, in the case of $a$ nuclei with a predominant $l=0$ intercluster motion, such momenta populate the high-momentum tail of the momentum distribution for particle $x$, making very difficult the separation of TH mechanism from eventual background reaction mechanisms, like sequential decays feeding the same exit channel.

However, one of us (C. Spitaleri) suggested a modification of THM, making it workable by noting that the initial projectile velocity can be compensated by the binding energy $\varepsilon_{sx}$ of the nucleus $a$ [36]. It can easily be seen if we take into account the energy-momentum conservation law for the virtual decay $a\rightarrow x+s$ and binary subprocess $A+x\rightarrow c+C$ in the TH reaction. Assuming that the TH reaction mechanism is described by the pole diagram 1 a we get [15]

$$E_{Ax}=\frac{p_{Ax}^2}{2\,\mu_{Ax}}-\frac{p_{sx}^2}{2\mu_{sx}}-\varepsilon_{sx}. \qquad (7)$$

In the QF kinematics $p_{sx}=0$ and Eq. (7) reduces to

$$E_{Ax}=\frac{m_x}{m_x+m_A}E_A-\varepsilon_{sx}. \qquad (8)$$

This equation explains why in the THM the binary reaction can be induced at very low energies $E_{Ax}$. Even if the energy of projectile $A$ exceeds the Coulomb barrier in the initial $A+a$ channel of the TH reaction, due to the smallness of the mass ratio factor $\frac{m_x}{m_x+m_A}$ and the presence of the $-\varepsilon_{sx}$, the relative

energy of the fragments in the initial channel $A + x$ of the binary reaction (2) can be very low and even negative.

In this way it is possible to extract the two-body cross section for a finite energy range from Eq. (9) after inserting the appropriate penetration function $G_l$ to account for the penetrability effects affecting the direct data below the Coulomb barrier [6,9]. The $[(d\sigma/d\Omega)_{\text{c.m.}}]^{\text{HOES}}$, extracted by means of THM, can be compared with direct data via the following equation:

$$\left(\frac{d\sigma}{d\Omega}\right) \propto \left(\frac{d^3\sigma}{dE_c d\Omega_c d\Omega_C}\right) \cdot [KF|\varphi(\mathbf{p}_s)|^2]^{-1} \cdot G_l, \qquad (9)$$

where we assume that only one orbital angular momentum $l$ in the subsystem $A + x$ contributes to the TH reaction. As shown above, because in the experimental works the IA validity conditions are fulfilled, the PWIA was applied for the extractions of the two-body cross section. The THM data are not affected by electron screening effects. Therefore, by comparing the $S(E)$ factor extracted from the TH reaction with the one obtained from direct measurements, we can determine the screening potential $U_e$. Then, after normalization of the indirect data to the direct ones, the comparison between the two data sets can be performed down to the low-energy region.

## III. MOMENTUM DISTRIBUTIONS

### A. Final-state interaction and momentum distribution of the spectator

There are different tests of the validity of the THM. One of the important tests is the comparison of the momentum distribution of the spectator extracted from the TH data with the momentum distribution of the spectator inside the TH particle $a$. Agreement of both distributions would be a strong indication of the validity of the impulse approximation used in the THM. On the contrary, a possible deviation of two distributions might indicate the onset of the interaction of the spectator with the final-state fragments $c$ and $C$ of reaction (1). Here we qualitatively discuss how the final-state interaction (FSI) can distort the momentum distribution of the spectator. Let us write down the amplitude of the TH process (1) in the following simplified form leaving two variables only

$$\begin{aligned} f(p_s, q_t) &= f_1(p_s, q_t) + f_2(p_s, q_t) \\ &= f_1(p_s, q_t)[1 + g(p_s, q_t)], \end{aligned} \qquad (10)$$

$$g(p_s, q_t) = \frac{f_2(p_s, q_t)}{f_1(p_s, q_t)}, \qquad (11)$$

where $f_1(p_s, q_t)$ is the amplitude of the pole diagram, Fig. 1(a) and $f_2(p_s, q_t)$ is the amplitude of the triangle diagram, Fig. 1(b), which describes the FSI, and $q_t$ is the transfer momentum from particle $A$ to the system $B = c + C$ determined as the Galilean invariant transferred momentum

$$\mathbf{q}_t = \left(\frac{m_B}{m_A}\right)^{1/2} \mathbf{p}_A - \left(\frac{m_A}{m_B}\right)^{1/2} \mathbf{p}_B \qquad (12)$$

from the projectile $A$ to the center-of-mass of the final system $B = C + c$. Because $\mathbf{q}_t$ is invariant we can easily derive the expression for $q_t$ in the QF kinematics. In the system where the TH particle $a$ is at rest, $p_a = 0$, in the QF kinematics also $p_s = 0$ and $\mathbf{p}_B = \mathbf{p}_A$. It reduces $\mathbf{q}_t$ in the QF kinematics to

$$\mathbf{q}_t^{\text{QF}} = m_x \sqrt{\frac{1}{m_A m_B}}\, \mathbf{p}_A \qquad (13)$$

or

$$q_t^{\text{QF}} = m_x \sqrt{\frac{2E_A}{m_B}}. \qquad (14)$$

It is known that the FSI usually diminishes the cross sections, hence $f_1(p_s, q_t)$ and $f_2(p_s, q_t)$ interfere destructively and the correction term $g(p_s, q_t)$ (or its real part) is negative. Consider first the behavior of $f(p_s, q_t)$ when $p_s$ varies at fixed $q_t$. It is known that the amplitude of the triangle diagram varies more slowly than that of the pole one [37]. It is true for skeleton diagrams, that is, for diagrams with constant vertex parts [37]. Because the three-ray vertex part $a \to s + x$ decreases sharply with $p_s$ increasing, it is even more true, because in the triangle diagram this vertex is integrated. The four-ray vertex parts describing $2 \to 2$ particles processes in the diagram vary more slowly than the vertex part $a \to s + x$. Moreover, the upper four-ray vertex in Fig. 1(b) is integrated and the lower four-ray vertex parts in Figs. 1(a) and 1(b) are canceled out in the expression for $g(p_s, q_t)$ (if one neglects the off-shell effects). Hence with increasing of $p_s$ the modulus of $g(p_s, q_t)$ will increase and, due to the destructive interference, the function $1 + g(p_s, q_t)$ in Eq. (10) will decrease. As a result, $f(p_s, q_t)$ will decrease more sharply than $f_1(p_s, q_t)$ what may effectively be interpreted as the narrowing of the $p_s$ distribution in $a$.

Consider now the behavior of $f(p_s, q_t)$ when $q_t$ varies at fixed $p_s$. If $p_s$ is constant, the pole amplitude $f_1(p_s, q_t)$ entering the ratio $g(p_s, q_t)$ can be considered as a constant [assuming that the lower four-ray vertices $2 \to 2$ particles in Figs. 1(a) and 1(b) are canceled out in the expression for $g(p_s, q_t)$]. However, the triangle amplitude $f_2(p_s, q_t)$ decreases with increasing of $q_t$. It follows both from the structure of the triangle diagram and from the known fact that the role of the FSI diminishes when the energy increases (in the QF kinematics the $q_t^2 \propto E_A$). Thus $f(p_s, q_t)$ approaches $f_1(p_s, q_t)$ with increasing of $q_t$ and the distribution in $p_s$ extracted from the TH reaction is expected to approach that corresponding to the pure pole mechanism. In what follows we will demonstrate it for different systems.

### B. Experimental momentum distributions

The results of the work [38] have been recently updated [14] because of the importance of weakly bound nuclei in the framework of the THM and its application to the nuclear astrophysics. Because the extraction of the bare-nucleus S(E) factor uses the momentum distribution of the spectator cluster inside the TH nucleus, it is important to evaluate the impact of the uncertainty of the momentum distribution width on the final result.

It has been shown [39] that the main features in the shape of momentum distributions for spectator momenta

smaller than 50 MeV/$c$, calculated in PWIA or distorted-wave impulse approximation (DWIA), are essentially the same. The PWIA has then been widely used because of its simplicity and because it predicts reasonably well the shape of the experimental momentum distribution in the region away from its zeros [39]. Because in TH applications within the QF region one generally selects events with low spectator momentum (in the system where $p_a = 0$), this approximation is well justified.

The goal of this article is to compare the experimental momentum distribution of the spectator in the bound state $a = (xs)$ extracted from the $2 \rightarrow 3$ particles (breakup or breakup with rearrangement) reactions with the theoretical one. The theoretical momentum distribution has been calculated for the target $a = (sx)$ using the Hulthen potential for $a = d$ and Woods-Saxon one with the standard geometrical parameters, radius $r_0 = 1.25$ fm and diffuseness $a = 0.65$ fm, for other nuclei.

In previous works [14,38] it has been shown that the full width at half maximum, $W(q_t)$, for the $\alpha$-$d$ momentum distribution in $^6$Li slowly increases with increasing mean transferred momentum. We will extend this study to the deuteron case as well as to other nuclides to determine at what conditions the PWIA works. The PWIA is described by the pole diagram Fig. 1(a). This is called the pole diagram because it contains the Fourier transform of the bound-state wave function of $a = (sx)$, which can be written, when one of the fragments is neutral, as $\varphi_a(\mathbf{p}_{sx}) = \frac{G(\mathbf{p}_{sx})}{p_{sx}^2 + \kappa_{sx}^2}$, where $\kappa_{sx} = \sqrt{2 \cdot \mu\, \varepsilon_{sx}}$, $\varepsilon_{sx}$ is the binding energy of the fragments $x$ and $s$ in the bound state $a = (sx)$ and $\mu$ is their reduced mass. Hence it has a pole at $p_{sx}^2 = -\kappa_{sx}^2$. Here $G(\mathbf{p}_{sx}) = \langle e^{i\,\mathbf{p}_{sx}\cdot\mathbf{r}} | V_{sx} | \varphi_{sx}(\mathbf{r}) \rangle$ is the form factor that is regular at $p_{sx}^2 = -\kappa_{sx}^2$. However, for charged particles $\varphi_a(\mathbf{p}_{\mathrm{sx}})$ has a branching point rather than the pole at $p_{sx}^2 = -\kappa_{sx}^2$.

When the final-state interaction is important, what can happen if, for example, the relative $s - c$ kinetic energy $E_{sc}$ (or $E_{sC}$) is small, the diagram describing the process is shown in Fig. 1(b). In this case one may expect the failure of the PWIA and deviation of the experimental momentum distribution from the theoretical one. In this article we compare the experimental momentum distribution of the spectator with the theoretical one at different projectile and ejectile energies and transfer momenta to check whether the PWIA is adequate. We will demonstrate that the applicability of the PWIA depends on the kinematical conditions of the experiment and reaction mechanism.

The standard procedure for the extraction of the momentum distribution from the experimental data is described in Ref. [11]. It follows from Eq. (3) that the PWIA allows us to directly relate the three-body differential cross section to the spectator momentum distribution $|\varphi(\mathbf{p}_s)|^2$. KF can be easily calculated. The energy behavior of $(\frac{d\sigma}{d\Omega}_{\mathrm{c.m.}})^{\mathrm{HOES}}$, which is the quantity one wants to obtain in TH applications, is generally not known. To obtain the momentum distribution from Eq. (3) the coincidence events in the $E_{Cc}$ vs. $p_s$ plot (see Fig. 2) in the TH experiment are chosen to cover a narrow angular and energy range (~50/100 keV). When projected onto the $p_s$ axis, $\frac{d\sigma}{d\Omega}_{\mathrm{c.m.}}^{\mathrm{HOES}}$ for those events is nearly constant.

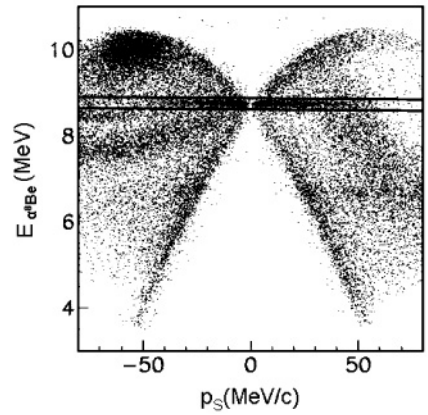


FIG. 2. Quasifree energy $E_{\alpha\,^8\mathrm{Be}}$ as a function of the spectator momentum $p_s$ for the $^2$H($^{11}$B,$\alpha^8$Be)$n$ reaction. A narrow cut was used for extraction of the momentum distribution as explained in the text.

Then dividing the triple differential cross section by the kinematical factor one obtains directly the shape of the experimental momentum distribution in arbitrary units in the PWIA.

### C. $^2$H as ($p\,n$)

The experimental results for the neutron-spectator momentum distribution as functions of $p_s$ obtained from the $^2$H($p,pp$)$n$ reaction at the projectile energy $E_0 = 5$ MeV (in the Lab system) [40] are shown in Fig. 3(a). In this case $a = d$, $s = n$, $x = p$, $A = p$, and $C = c = p$. In the QF kinematics ($p_s = 0$) we select the events corresponding to the kinetic energies of the ejectiles $E_C = 1.4$ MeV and $E_c = 1.37$ MeV. The relative energies $C - s$ and $c - s$ are ≈0.7 MeV. The theoretical prediction of the spectator-neutron momentum distribution has been obtained using the Fourier transform of the Hulthen $d = (pn)$ bound-state wave function [12]:

$$\varphi(\mathbf{p}_s) = \frac{1}{\pi}\sqrt{\frac{ab(a+b)}{(a-b)^2}}\left(\frac{1}{a^2+p_s^2} - \frac{1}{b^2+p_s^2}\right), \quad (15)$$

with parameters $a = 0.2317$ fm$^{-1}$ and $b = 1.202$ fm$^{-1}$ [12] for the deuteron ground state.

To determine the momentum distribution shown in Fig. 3(a), which covers the interval $p_s \leqslant 60$ MeV/$c$, we also select the events away from the QF kinematics keeping $q_t \approx 40$ MeV/$c$. Because the experimental data were obtained in arbitrary units in all the cases considered in the article we normalized the experimental data to the theoretical momentum distribution at $p_s = 0$. One sees the PWIA is not satisfactory, i.e., the final-state interactions $p - n$ are not negligible due to the small relative $E_{pn}$ energies.

In Fig. 3(b) similar results are shown for the neutron-spectator momentum distribution from the $^2$H($^{11}$B,$\alpha^8$Be)$n$ reaction at the projectile $A = {}^{11}$B energy $E_0 = 27$ MeV [11]. In this case $a = d$, $s = n$, $x = p$, $C = {}^8$Be, and $c = \alpha$. In the QF kinematics ($p_s = 0$) the kinetic energies of the ejectiles

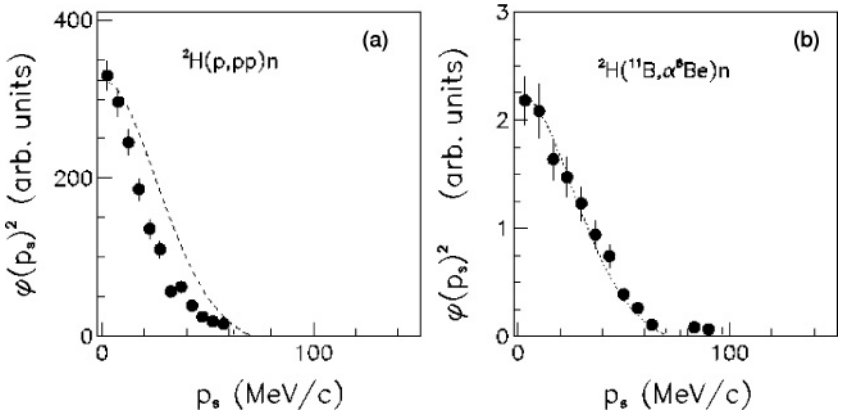


FIG. 3. Experimental momentum distribution for the proton inside deuteron derived according to the method explained in the text for the $^2\mathrm{H}(p,pp)n$ (a) and $^2\mathrm{H}(^{11}\mathrm{B}\alpha^8\mathrm{Be})n$ (b) reactions. The squared Hulthen function in momentum space is superimposed to data.

are $E_C = 8.5$ MeV and $E_c = 25$ MeV. The selected events correspond to the relative energies $E_{Cs} = 1$ MeV and $E_{cs} = 5$ MeV. Despite the low relative energy $E_{Cs}$ the experimental momentum distribution agrees very well with the theoretical one, i.e., the PWIA works quite well. The reason is presumably in the reaction mechanism: the subreaction $^{11}\mathrm{B}(p,\alpha)^8\mathrm{Be}$ proceeds through the narrow resonance so, when it decays, its products and neutron are well separated and distortion of the neutron momentum distribution due to the final-state interaction is diminished. The momentum distribution shown in Fig. 3(b) covers the region $p_s < 100$ MeV/$c$ and correspond to the events with the transfer momentum $q_t \approx 210$ MeV/$c$. High transfer momenta confirm the result [14] that the PWIA works better with increasing of the transfer momentum.

The experimental momentum distribution FWHM $W(q_t)$, extracted from several experiments, are reported together with the transferred momentum calculation and references in Table II. Moreover, other data were taken from literature [16,17,41,42]. The complete data set is plotted in Fig. 4 as a function of the transferred momentum, defined above.

Previous data extracted from several studies [16,17,41,42] are presented as empty crosses while our recent results from several different experiments and energies (see Table II) [8–12] are shown as full dots. Also in this case it is evident how, at low $q_t$, the $W_t$ smoothly increases until the predicted PWIA asymptotic value (around 60 MeV/$c$) is reached in the region where $q_t$ is 200 MeV/$c$. These data strongly confirm the behavior already discussed in Refs. [14,38] for the $\alpha$-$d$ case in $^6$Li and reported in Fig. 5.

This experimental behavior was fitted by using the following empirical function, as in [14]:

$$W(q_t) = f_0[1 - \exp(-q_t/q_0)] \tag{16}$$

and yields an asymptotic width value of $f_0 = 58$ MeV/$c$ and $q_0 = 60 \pm 12$ MeV/$c$.

TABLE II. Transferred momentum for different reactions and beam energies together with the measured width (FWHM) for deuterium momentum distribution.

| Reaction | $E_{\mathrm{beam}}$ (MeV) | $q_t$ (MeV/$c$) | W($q_t$) (MeV/$c$) | Ref. |
|---|---|---|---|---|
| $^2\mathrm{H}(p,pp)n$ | 6 | 51 | 46 | [40] |
| $^2\mathrm{H}(p,pp)n$ | 5 | 39 | 42 | [40] |
| $^2\mathrm{H}(t,tp)n$ | 35.5 | 140 | 58 | [23] |
| $^2\mathrm{H}(^6\mathrm{Li},\alpha^3\mathrm{He})n$ | 25 | 230 | 57 | [10] |
| $^2\mathrm{H}(^9\mathrm{Be},\alpha^6\mathrm{Li})n$ | 22 | 190 | 54 | [25] |
| $^2\mathrm{H}(^{10}\mathrm{B},\alpha^7\mathrm{Be})n$ | 27 | 188 | 58 | [26] |
| $^2\mathrm{H}(^{11}\mathrm{B},\alpha_0^8\mathrm{Be})n$ | 27 | 210 | 60 | [11] |
| $^2\mathrm{H}(^7\mathrm{Li},\alpha\alpha)n$ | 20 | 194 | 55 | [9] |
| $^2\mathrm{H}(^{15}\mathrm{N},\alpha^{12}\mathrm{C})n$ | 60 | 273 | 56 | [43] |
| $^2\mathrm{H}(^{18}\mathrm{O},\alpha^{15}\mathrm{N})n$ | 54 | 301 | 58 | [27] |

### D. $^6$Li as ($\alpha$ $d$)

The experimental results for the $\alpha$ spectator momentum distribution as functions of $p_s$ obtained from the $^6\mathrm{Li}(^6\mathrm{Li},\alpha\alpha)^4\mathrm{He}$ reaction at the projectile energy $E_0 = 3.6$ MeV are shown in Fig. 6(a). In this case $a = {}^6\mathrm{Li}$, $s = \alpha$, $x = d$, $A = {}^6\mathrm{Li}$, and $C = c = \alpha$. In the QF kinematics ($p_s = 0$) the kinetic energies of the ejectiles are $E_C = 14$ MeV and $E_c = 8$ MeV. The relative energies $C - s$ and $c - s$ are $\approx$7 and 4 MeV, respectively. The theoretical prediction of the spectator momentum distribution has been obtained using the Woods-Saxon potential with the standard geometrical parameters, as stated above.

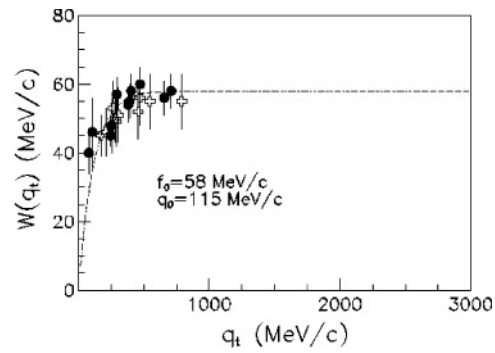


FIG. 4. Width (FWHM) for the momentum distribution of the proton inside deuteron as a function of the transferred momentum $q_t$. Open symbols represent previous results by Refs. [16,17,41,42], full dots are new data from different experiments reported in Table III. The line represents an empirical fit described in the text.

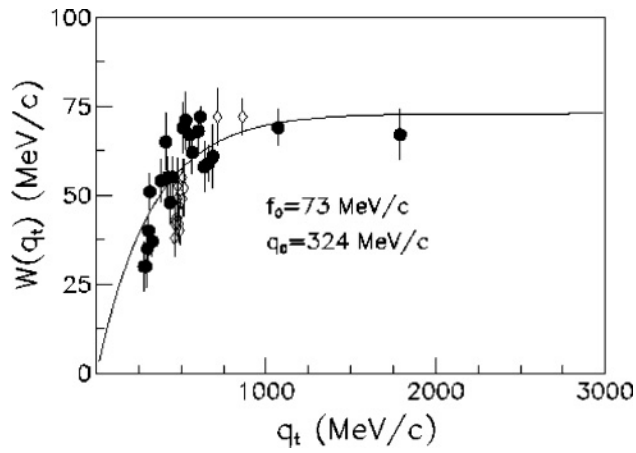


FIG. 5. Width (FWHM) for the momentum distribution of the $\alpha$ particle inside $^6$Li as a function of the transferred momentum $q_t$. Data are taken from the case discussed in Ref. [14]. The line represents an empirical fit described in the text.

TABLE III. Transferred momentum for different reactions and beam energies together with the measured width (FWHM) for $^6$Li momentum distribution.

| Reaction | $E_{\text{beam}}$ (MeV) | $q$ (MeV/$c$) | W($q_t$) (MeV/$c$) | Ref. |
|---|---|---|---|---|
| $^6$Li($^6$Li,$\alpha\alpha$)$^4$He | 2.1 | 225 | $49 \pm 5$ | |
| | 2.7 | 236 | $43 \pm 4$ | |
| | 2.7 | 240 | $53 \pm 4$ | |
| | 3.6 | 256 | $40 \pm 5$ | [24] |
| | 4.7 | 241 | $45 \pm 5$ | [24] |
| | 5.7 | 253 | $49 \pm 5$ | [24] |
| | 5.9 | 270 | $61 \pm 5$ | [7] |
| | 6.7 | 241 | $63 \pm 5$ | [24] |
| | 44 | 400 | $72 \pm 15$ | |
| $^3$He($^6$Li,$p\alpha$)$^4$He | 5 | 460 | $40 \pm 3$ | [28] |
| | 6 | 508 | $55 \pm 3$ | [28] |

The momentum distribution shown in Fig. 6 a covers the interval $p_s < 60$ MeV/$c$ and corresponds to the events with $q_t \approx 250$ MeV/$c$. As we can see the agreement with PWIA is not satisfactory. In Fig. 6(b) similar results are shown for the $\alpha$-spectator momentum distribution from the same reaction at the projectile energy $E_0 = 5.9$ MeV [7]. In this case $a = {}^6$Li, $s = \alpha, x = d$, $A = {}^6$Li, and $C = c = \alpha$. In the QF kinematics ($p_s = 0$) we select the events with the kinetic energies of the ejectiles $E_C = 15$ MeV and $E_c = 12$ MeV. The relative energies are $E_{Cs} = 7.5$ MeV and $E_{cs} = 6$ MeV. The experimental momentum distribution, which covers the region $p_s < 80$ MeV/$c$ and corresponds to the events with the transfer momentum $q_t = 280$ MeV/$c$, agrees very well with the theoretical one, i.e., the PWIA works quite well. In this case higher transfer momenta confirm the result [14] that the PWIA works better with increasing of the transfer momentum.

Data from several experiments using the $^6$Li $= (\alpha d)$ cluster structure were extracted. They are shown together with the transferred momentum calculation and references in Table III. All these data are reported extensively in Refs. [14,38]. It is evident how, at low $q_t$, the momentum distribution full width, $W_t$, smoothly increases until the predicted PWIA asymptotic value (around 73 MeV/$c$) is reached in the region where $q_t$ is large. These data strongly confirm the behavior already discussed in Ref. [38] and are reported in Fig. 5. This experimental behavior was fitted using Eq. (16) with $f_0 = 73$ MeV/$c$ and $q_0 = 120 \pm 14$ MeV/$c$.

### E. $^3$He as ($pd$)

The experimental results for the proton spectator momentum distribution as functions of $p_s$ obtained from the $^2$H($^3$He, $p^3$H)H reaction at the projectile energy $E_0 = 17$ MeV are shown in Fig. 7(a). In this case $a = {}^3$He, $s = p, x = d$, $A = {}^2$H, $C = {}^3$H, and $c = p$. In the QF kinematics ($p_s = 0$) the selected kinetic energies of the ejectiles are $E_C = 4$ MeV and $E_c = 7.5$ MeV. The relative energies $C - s$ and $c - s$ are $\approx$3.5 and 1 MeV, respectively. The theoretical prediction of the spectator momentum distribution has been obtained using the Woods-Saxon potential with the standard geometrical parameters, as in the previous case.

The momentum distribution shown in Fig. 7, which covers the interval $p_s < 50$ MeV/$c$ and corresponds to the transfer momentum $q_t \approx 120$ MeV/$c$, demonstrates a complete failure of the PWIA. In Fig. 7(b) similar results are shown

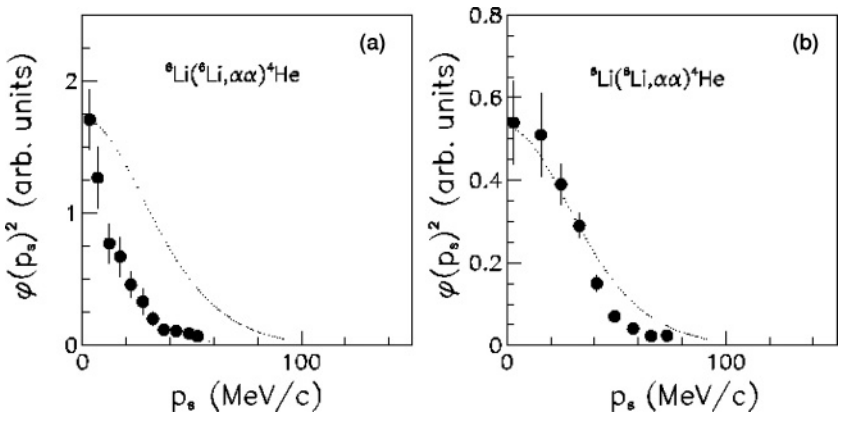


FIG. 6. Experimental momentum distribution for $d$ inside $^6$Li for the $^6$Li($^6$Li,$\alpha\alpha$)$^4$He reaction at 3.6 (a) and 5.9 MeV (b). Dashed line is the theoretical one discussed in the text.

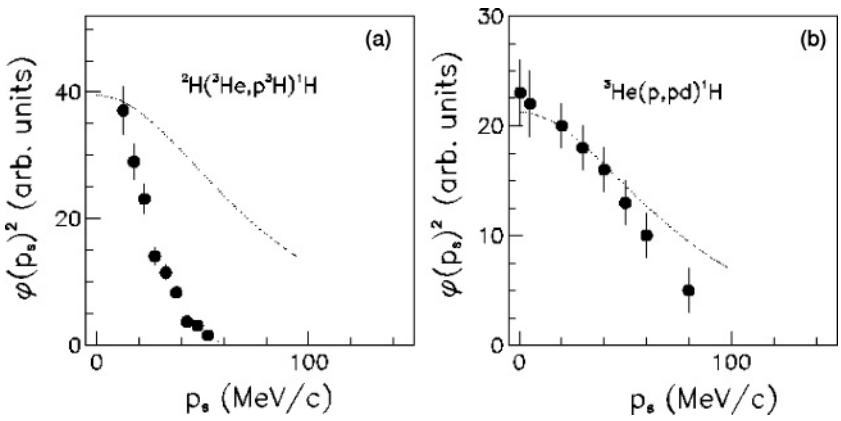


FIG. 7. Experimental momentum distribution for $p$ in $^3$He for the $^2$H($^3$He, $p^3$He)$n$ reaction at 17 MeV (a) and the $^3$He$(p, pd)$H at 100 MeV (b). Line is the theoretical prediction discussed in the text.

for the proton-spectator momentum distribution from the $^3$He$(p, pd)$H reaction at the projectile energy $E_0 = 100$ MeV [21]. The selected events correspond to the transfer momentum $q_t \approx 375$ MeV/$c$ and cover the interval $p_s \leqslant 80$ MeV/$c$. In this case $a = {}^3$He, $s = p$, $x = d$, $A = p, C = d$, and $c = p$. In the QF kinematics ($p_s = 0$) the selected kinetic energies of the ejectiles $E_C = 47$ MeV and $E_c = 47.5$ MeV are significantly higher than those in the previous case. The relative energies $E_{Cs} \approx 16$ MeV and $E_{cs} \approx 24$ MeV are also higher. The experimental momentum distribution agrees very well with the theoretical one, i.e., the PWIA works quite well, confirming the result [14] that the PWIA works better with increasing of the transfer momentum.

Data from several experiments using the $^3$He $= (pd)$ cluster structure were extracted and are shown together with the transferred momentum calculation and references in Table IV. Also in this case it is evident that $W_t$ smoothly increases with $q_t$ until the predicted PWIA asymptotic value (around 110 MeV/$c$) is reached but at a significantly higher value of $q_t \approx 500 - 600$ MeV/$c$ (see Fig. 8) than what can be explained by the higher $\kappa_{sx}$ compared to the previous cases (see Table V). This experimental behavior was fitted using Eq. (16) with $f_0 = 110$ MeV/$c$ and $q_0 = 270 \pm 20$ MeV/$c$.

TABLE IV. Transferred momentum for different reactions and beam energies together with the measured width (FWHM) for $^3$He.

| Reaction | $E_{\text{beam}}$ (MeV) | $q_t$ (MeV/$c$) | W($q_t$) (MeV/$c$) | Ref. |
|---|---|---|---|---|
| $^7$Li($^3$He,$\alpha\alpha$)$^2$H | 11 | 115 | $56 \pm 8$ | [19] |
| $^3$He$(d, pt)$H | 17 | 120 | $40 \pm 8$ | |
| $^3$He$(d, p^3$He)n | 18 | 145 | $38 \pm 9$ | |
| $^7$Li($^3$He,$\alpha\alpha$)$^2$H | 12 | 160 | $55 \pm 8$ | [19] |
| $^3$He$(d, pt)$H | 35 | 200 | $61 \pm 10$ | [20] |
| $^7$Li($^3$He,$\alpha\alpha$)$^2$H | 33 | 260 | $70 \pm 8$ | [45] |
| $^3$He$(d, pt)$H | 52 | 230 | 60 | [20] |
| $^3$He$(p, pd)$H | 65 | 130 | 73 | [21] |
| $^3$He$(p, pd)$H | 85 | 340 | 78 | [21] |
| $^3$He$(p, pd)$H | 100 | 375 | 86 | [21] |
| $^3$He$(p, pd)$H | 590 | 582 | 110 | [22] |

### F. $^9$Be as ($\alpha$ $^5$He)

The experimental results for the $^5$He spectator momentum distribution as functions of $p_s$ obtained from the $^9$Be$(p, p\alpha)^5$He reaction at the projectile energy $E_0 = 47$ MeV [44] are shown in Fig. 9(a). In this case $a = {}^9$Be, $s = {}^5$He, $x = \alpha$, $A = p$, $C = \alpha$, and $c = p$. In the QF kinematics the selected kinetic energies of the ejectiles are $E_C = 11$ MeV and $E_c = 40$ MeV. The relative energies $C - s$ and $c - s$ are $\approx$5 and 30 MeV, respectively. The theoretical prediction of the spectator momentum distribution has been obtained using the Woods-Saxon potential with the standard geometrical parameters, as in previous cases.

The experimental momentum distribution obtained from the events corresponding to the transfer momentum $q_t = 470$ MeV/$c$. As we can see the agreement with PWIA is not satisfactory. It is worth mentioning that we observed a similar failure of the PWIA in the case of the $^6$Li($^6$Li,$\alpha\,\alpha$)$^4$He at $E_0 = 3.6$ MeV, where the relative energy $E_{\alpha-\alpha} = 5$ MeV was kind of the border for PWIA to be applicable.

In Fig. 9(b) similar results are shown for the spectator momentum distribution from the $^9$Be($^7$Li, $^7$Li$\alpha$)$^5$He reaction at the projectile energy $E_0 = 52$ MeV [33]. The selected events correspond to the transfer momentum $q_t \approx 650$ MeV/$c$. In this case $a = {}^9$Be, $s = {}^5$He, $x = \alpha$, $A = {}^7$Li, $C = {}^7$Li, and $c = \alpha$. In the QF kinematics the selected kinetic energies of the ejectiles are $E_C = 25$ MeV and $E_c = 25$ MeV. The relative energies are $E_{Cs} \approx 13.5$ MeV and $E_{cs} \approx 10$ MeV. We can see that for the case under consideration the PWIA works quite well.

Data from several experiments using the $^9$Be $= (\alpha^5$He) cluster structure were extracted and are shown together with

TABLE V. Parameters obtained for Eq. (16).

| Nucleus | $\kappa_{sx}$ (MeV/$c$) | $q_0$ (MeV/$c$) | $f_0$ (MeV/$c$) |
|---|---|---|---|
| $^2$H | 45.8 | $60 \pm 12$ | 58 |
| $^6$Li | 60.5 | $120 \pm 14$ | 73 |
| $^3$He | 82.5 | $270 \pm 20$ | 110 |
| $^3$H | 88 | $350 \pm 35$ | 110 |
| $^9$Be | 99.7 | $405 \pm 30$ | 115 |

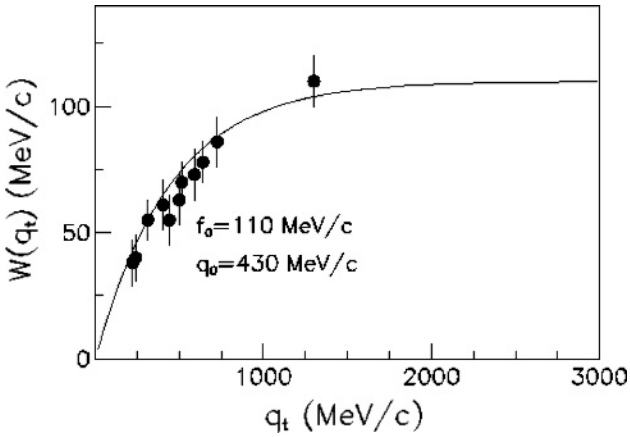


FIG. 8. Width (FWHM) for the momentum distribution of the $p$ inside $^3$He as a function of the transferred momentum $q_t$. The solid line represents an empirical fit described in the text.

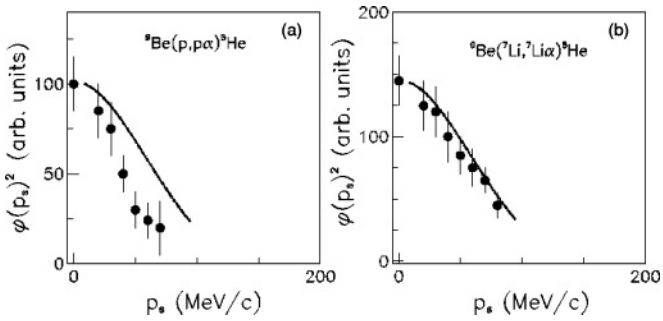


FIG. 9. Experimental momentum distribution for $^4$He in $^9$Be for the $^9$Be$(p, p\alpha)^5$He reaction at 47 MeV (a) and the $^9$Be$(^7$Li, $^7$Li$\alpha)^5$He at 52 MeV (b). The solid line is the theoretical prediction as discussed in the text.

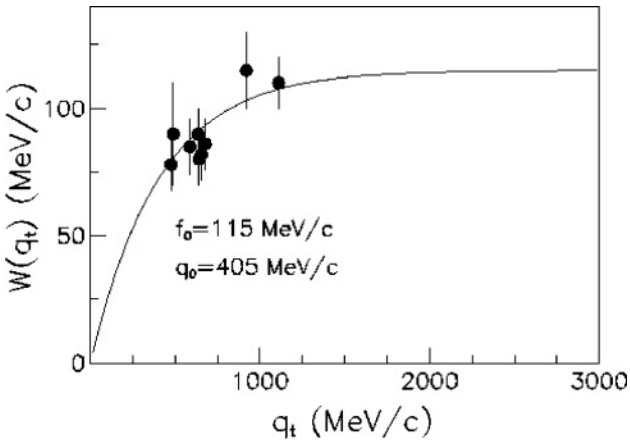


FIG. 10. Width (FWHM) of the momentum distribution of the $\alpha$ inside $^9$Be as a function of the transferred momentum $q_t$. The line represents an empirical fit described in the text.

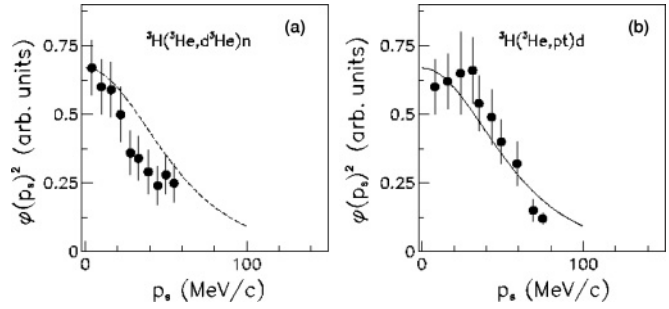


FIG. 11. Experimental momentum distribution for $^2$H in $^3$H for the $^3$H$(^3$He, $d^3$He$)n$ reaction at 65 MeV (a) and $^3$H$(^3$He, $pt)^2$H reaction at 78 MeV as reported in Ref. [46] (b). The square of the wave function in the momentum space (Hulthen function) [47] is shown as a solid line.

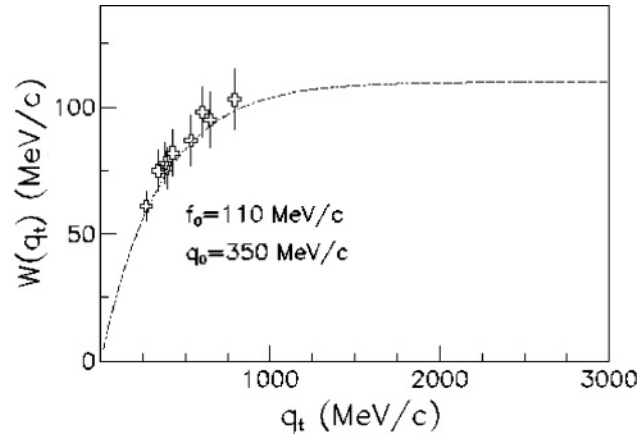


FIG. 12. Width (FWHM) of the momentum distribution of the $d$ inside $^3$H as a function of the transferred momentum $q_t$. The line represents an empirical fit described in the text.

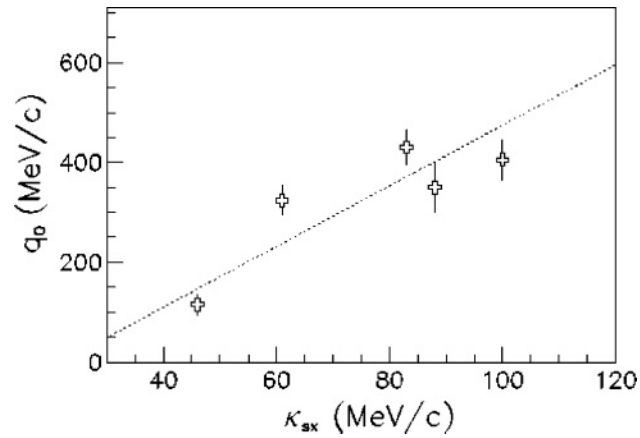


FIG. 13. Correlation between $q_0$ and $\kappa_{sx}$ as discussed in the text. A linear regression is superimposed to the experimental points.

TABLE VI. Transferred momentum for different reactions and beam energies together with the measured width (FWHM) for $^9$Be.

| Reaction | $E_{\rm beam}$ (MeV) | $q_t$ (MeV/$c$) | W($q_t$) (MeV/$c$) | Ref. |
|---|---|---|---|---|
| $^9$Be($p,p\alpha$)$^5$He | 47 | 470 | $89 \pm 10$ | [44] |
| $^9$Be($p,p\alpha$)$^5$He | 55 | 655 | $82 \pm 20$ | [29] |
| $^9$Be($p,p\alpha$)$^5$He | 57 | 580 | $85 \pm 10$ | [48] |
| $^9$Be($^3$He,$\alpha\alpha$)$^4$He | 4 | 470 | $78 \pm 10$ | [18,31] |
| $^9$Be($^3$He,$\alpha\alpha$)$^4$He | 2.8 | 635 | $90 \pm 10$ | [30] |
| $^9$Be($p,d\alpha$)$^4$He | 30 | 640 | $80 \pm 10$ | [31] |
| $^9$Be($^3$He,$\alpha\alpha$)$^4$He | 3 | 655 | $80 \pm 10$ | [32] |
| $^9$Be($p,p\alpha$)$^5$He | 160 | 920 | $100 \pm 15$ | [44] |
| $^9$Be($^7$Li,$^7$Li$\alpha$)$^5$He | 52 | 650 | $100 \pm 10$ | [33] |
| $^9$Be($\alpha,\alpha\alpha$)$^5$He | 140 | 1110 | $106 \pm 10$ | [49] |

the transferred momentum calculation and references in Table VI. They all are plotted in Fig. 10 as a function of the transferred momentum defined above. The plateau in $W_t$ is reached in the region $q_t \geqslant 1000$ MeV/$c$. This experimental behavior was fitted using Eq. (16) with $f_0 = 115$ MeV/$c$ and $q_0 = 405 \pm 30$ MeV/$c$.

### G. $^3$H as ($nd$)

Data studying the momentum distribution of $^3$H are quite scarce and the data sets available for the analysis are quite few. The experimental results for the spectator momentum distribution as functions of $p_s$ obtained from the $^3$H($^3$He, $d^3$He)$n$ reaction at the projectile energy $E_0 = 65$ MeV [46] are shown in Fig. 11(a). The selected events correspond to the transferred momentum $q_t = 396$ MeV/$c$. In this case $a = {}^3$H, $s = n$, $x = d$, $A = {}^3$He, $C = d$, and $c = {}^3$He. In the QF kinematics ($p_s = 0$) the selected kinetic energies of the ejectiles are $E_C = 27$ MeV and $E_c = 30$ MeV. The relative energies $C - s$ and $c - s$ are ≈9 and 7.5 MeV, respectively. The theoretical prediction of the spectator-neutron momentum distribution has been obtained using the square of the wave function in momentum space [47]. As we can see the agreement with the PWIA is not satisfactory.

In Fig. 11(b) similar results are shown for the deuteron spectator momentum distribution from the $^3$H($^3$He, $pt$)$^2$H reaction at the projectile energy $E_0 = 78$ MeV [45]. The selected events correspond to the transfer momentum $q_t \approx 550$ MeV/$c$. We note that the peak is not centered, as in the other examined cases, at $p_s = 0$, what can be the result of experimental uncertainties. In this case $a = {}^3$H, $s = d, x = n$, $A = {}^3$He, $C = t$, and $c = p$. In the QF kinematics ($p_s = 0$) the selected kinetic energies of the ejectiles are $E_C = 37$ MeV and $E_c = 35$ MeV. The relative energies are $E_{Cs} \approx 13.8$ MeV and $E_{cs} \approx 23.5$ MeV. The experimental momentum distribution agrees reasonably with the theoretical one, i.e., the PWIA works quite well.

In the case of the triton the correlation between the transferred momentum and the width of the momentum distribution yields similar results as for other light nuclei examined above. Data are shown in Table VII and are plotted in Fig. 12. The same function adopted for the other cases is used for the tritium case. In this case $q_0 = 350 \pm 35$ MeV/$c$ and $f_0 = 110$ MeV/$c$.

TABLE VII. Transferred momentum for different reactions and beam energies together with the measured width (FWHM) for $^3$H.

| Reaction | $E_{\rm beam}$ (MeV) | $q_t$ (MeV/$c$) | W($q_t$) (MeV/$c$) | Ref. |
|---|---|---|---|---|
| $^3$H($^3$He, $d^3$He)$n$ | 65 | 645 | 95 | [46] |
| $^3$H($^3$He, $p^3$He)$2n$ | 65 | 600 | 98 | [46] |
| $^3$H($^3$He, $dd$)$^2$H | 78 | 533 | 87 | [46] |
| $^3$H($^3$He, $pt$)$^2$H | 78 | 790 | 103 | [46] |
| $^3$H($^3$He, $dd$)$^2$H | 50 | 425 | 82 | [50] |
| $^3$H($d, dd$)$n$ | 35 | 380 | 78 | [50] |
| $^3$H($^3$He, $dd$)$^2$H | 65 | 390 | 76 | [46] |
| $^3$H($p, 2p$)$2n$ | 45.6 | 260 | 61 | [51] |
| $^3$H($p, pd$)$n$ | 45.6 | 330 | 75 | [51] |

## IV. CONCLUSIONS

What seems clear from this analysis is that as far as the energies of the ejectiles are large enough the momentum distribution of the spectator extracted from the experimental data using the PWIA agrees with the theoretical prediction calculated using the Fourier transform of the bound-state wave function of the Trojan horse nucleus. We found that the deviation of the theoretical momentum distributions from the experimental ones is correlated with the transfer momentum from the projectile to the ejectiles. When the average transferred momentum is large compared to $\kappa_{sx}$ the experimental FWHM reaches the theoretical one [the plateau is reached at $q_t \sim (5-6)\kappa_{sx}$] (see Table V). Thus at higher relative $C - s$ and $c - s$ kinetic energies and higher $q_t$ the final-state ejectile-spectator effects are negligible and the reaction is an "ideal" quasifree reaction. But as soon as the relative $C - s$ and $c - s$ kinetic energies decreases or the transferred momentum become comparable with $\kappa_{sx}$ the momentum distribution shape changes and its width becomes smaller. This behavior appears for all the examined nuclei, $^2$H, $^3$He,$^6$Li, $^3$H, and $^9$Be. The application of the THM to these cases should take into account these distortions by adopting the "distorted" FWHM extracted from the experimental data instead of the theoretical one. This shows even more clearly that the distortions are stronger with decreasing $E_{Cs}$, $E_{cs}$, or $q_t$ and could be parameterized by Eq. (16). Moreover, the onset of these effects depends on the examined nucleus. If we plot $q_0$ as a function of $\kappa_{sx}$, a linear behavior is found (see Fig. 13). A linear fit is performed and a linear regression gives:

$$q_0 = -239.16 + 6.3\kappa_{sx}. \quad (17)$$

According to the present results this trend is confirmed at least for the examined nuclei (all with $l = 0$ intercluster motion).

## ACKNOWLEDGMENTS

This work was supported in part by the US Department of Energy under Grant Nos. DE-FG02-93ER40773 and DE-FG52-06NA26207 and the NSF under Grant No. PHY-0852653.

[1] G. Baur, C. A. Bertulani, and H. Rebel, Nucl. Phys. **A458**, 188 (1986).
[2] X. Tang, A. Azhari, C. A. Gagliardi, A. M. Mukhamedzhanov, F. Pirlepesov, L. Trache, R. E. Tribble, V. Burjan, V. Kroha, and F. Carstiou, Phys. Rev. C **67**, 015804 (2003).
[3] A. M. Mukhamedzhanov, C. A. Gagliardi, and R. E. Tribble, Phys. Rev. C **63**, 024612 (2001).
[4] A. Azhari, V. Burjan, F. Carstoiu, C. A. Gagliardi, V. Kroha, A. M. Mukhamedzhanov, F. M. Nunes, X. Tang, L. Trache, and R. E. Tribble, Phys. Rev. C **63**, 055803 (2001).
[5] A. M. Mukhamedzhanov and R. E. Tribble, Phys. Rev. C **59**, 3418 (1999).
[6] S. Cherubini *et al.*, Ap. J. **457**, 855 (1996).
[7] C. Spitaleri *et al.*, Phys. Rev. C **63**, 055801 (2001).
[8] M. Lattuada *et al.*, Ap. J. **562**, 1076 (2001).
[9] C. Spitaleri *et al.*, Phys. Rev. C **60**, 055802 (1999).
[10] A. Tumino *et al.*, Phys. Rev. C **67**, 065803 (2003).
[11] C. Spitaleri *et al.*, Phys. Rev. C **69**, 055806 (2004).
[12] M. Zadro *et al.*, Phys. Rev. C **40**, 181 (1989).
[13] G. Calvi *et al.*, Nucl. Phys. **A621**, 139c (1997).
[14] R. G. Pizzone *et al.*, Phys. Rev. C **71**, 058801 (2005).
[15] M. La Cognata *et al.*, Phys. Rev. C **76**, 065804 (2007).
[16] D. J. Margaziotis *et al.*, Phys. Rev. C **2**, 2050 (1970).
[17] V. Valkovic *et al.*, Nucl. Phys. **A166**, 547 (1971).
[18] J. Kasagi, T. Nakagawa, N. Sekine, and T. Tohei, Nucl. Phys. **A239**, 233 (1975).
[19] M. Zadro, Dj. Miljanić, M. Lattuada, F. Riggi, and C. Spitaleri, Nucl. Phys. **A474**, 373 (1987).
[20] I. Slaus *et al.*, Nucl. Phys. **A286**, 67 (1977).
[21] A. Cowley *et al.*, Nucl. Phys. **A220**, 429 (1974).
[22] P. Kitching *et al.*, Phys. Rev. C **6**, 769 (1972).
[23] S. Blagus *et al.*, Z. Phys. A **337**, 297 (1990).
[24] M. Lattuada, F. Riggi, D. Vinciguerra, C. Spitaleri, G. Vourvopoulos, Đ. Miljanić, and E. Norbeck, Z. Phys. A-Atomic Nuclei **330**, 183 (1986).
[25] S. Romano *et al.*, EPJ. A. direct **27**, Supplement 1, 221 (2006).
[26] L. Lamia *et al.*, Nucl. Phys. **A787**, 309c (2007).
[27] M. La Cognata *et al.*, J. Phys. G: Nucl. Part. Phys. **35**, 014008 (2008).
[28] M. La Cognata *et al.*, Phys. Rev. C **72**, 065802 (2005).
[29] S. Yamashita *et al.*, J. Phys. Soc. Jpn. **26**, 1078 (1969).
[30] N. Arena *et al.*, Lett. Nuovo Cimento **17**, 231 (1976).
[31] M. Lattuada *et al.*, Nuovo Cimento **69**, 1 (1982).
[32] M. Lattuada *et al.*, Nucl. Phys. **A458**, 493 (1986).
[33] N. Soić *et al.*, Eur. Phys. J. A **3**, 303 (1998).
[34] G. Baur, Phys. Lett. **B178**, 135 (1986).
[35] G. Jacob and Th. A. Maris, Rev. Mod. Phys. **38**, 121 (1966).
[36] C. Spitaleri, *Problems of Fundamental Modern Physics II* (World Scientific, Singapore, 1990), pp. 21–35.
[37] L. Blokhintsev *et al.*, Nucl. Phys. **40**, 117 (1963).
[38] S. Barbarino, M. Lattuada, F. Riggi, C. Spitaleri, and D. Vinciguerra, Phys. Rev. C **21**, 1104 (1980).
[39] P. G. Roos *et al.*, Phys. Rev. C **15**, 69 (1977).
[40] A. Tumino *et al.*, Phys. Rev. Lett. **98**, 252502 (2007).
[41] J. Pan *et al.*, Nucl. Phys. **A150**, 216 (1970).
[42] J. M. Lambert, P. A. Treado, P. G. Roos, N. S. Chant, A. Nadasen, I. Slaus, and Y. Koike, Phys. Rev. C **26**, 357 (1982).
[43] M. La Cognata *et al.*, Eur. Phys. J. A **27**, s01, 249 (2006).
[44] H. J. Hoffman *et al.*, Nucl. Phys. **A210**, 126 (1973).
[45] A. Tumino *et al.*, Eur. Phys. J. A **27**, 243 (2006).
[46] J. M. Lambert *et al.*, Nucl. Phys. **A329**, 25 (1979).
[47] S. Blagus *et al.*, Phys. Rev. C **44**, 325 (1991).
[48] P. G. Roos *et al.*, Phys. Rev. **176**, 1246 (1968).
[49] C. W. Wang, N. S. Chant, P. G. Roos, A. Nadasen, and T. A. Carey, Phys. Rev. C **21**, 1705 (1980).
[50] I. Slaus *et al.*, Phys. Rev. C **8**, 444 (1973).
[51] D. I. Bonbright *et al.*, Phys. Rev. C **13**, 68 (1976).